Scales of variability of black carbon plumes over the Pacific Ocean

N. M. Weigum,[1] P. Stier,[1] J. P. Schwarz,[2,3] D. W. Fahey,[2,3] and J. R. Spackman[3,4]

Received 1 May 2012; revised 25 June 2012; accepted 2 July 2012; published 4 August 2012.

[1] Scales of spatial variability of black carbon (BC) aerosol plumes are quantified during the HIPPO aircraft campaign, which flew multiple missions from pole-to-pole over the Pacific ocean. During the first three missions of HIPPO, over 400 vertical profiles of BC concentrations were obtained using a Single Particle Soot Photometer (SP2). In this work, a total of 100 plumes are identified and analyzed. Due to the nature of the HIPPO flight track, the plume length scale is defined along the slanted flight track, having both vertical and horizontal components. These plumes comprise 57% of the total BC mass measured and have a median scale of 113 km. An analysis of BC variability based on autocorrelation functions confirms that most of BC's variability exists on scales similar to the majority of measured plume scales, with a range of 85–155 km. The plume scales are compared to an effective along-track global circulation model (GCM) resolution, which ranges from 20 km for low altitudes and steep ascents to 230 km for high altitudes and shallower ascents. The results suggest that plumes characterized predominantly by their horizontal variation at these scales are too small to be captured by GCMs running at resolutions currently suitable for climate simulations. **Citation:** Weigum, N. M., P. Stier, J. P. Schwarz, D. W. Fahey, and J. R. Spackman (2012), Scales of variability of black carbon plumes over the Pacific Ocean, *Geophys. Res. Lett.*, *39*, L15804, doi:10.1029/2012GL052127.

1. Introduction

[2] Black carbon (BC) is the major anthropogenic aerosol absorber of solar radiation. Model simulations have shown that, on average, BC absorption reduces anthropogenic aerosol top-of-atmosphere negative radiative forcing by 60% [*Schulz et al.*, 2006]. BC can also affect the Earth's radiation balance through a number of complex interactions with clouds and the Earth's surface, making its total effect highly uncertain [*Ramanathan and Carmichael*, 2008].

[3] Prediction of BC's effect on climate depends on the ability of global circulation models (GCM) to simulate its atmospheric concentrations and microphysical properties. However, models show large discrepancies (by factors of 2–4) in BC concentrations when compared to observations [e.g., *Koch et al.*, 2009; *Wang et al.*, 2011; *Bauer et al.*, 2010]. Uncertainties in model simulations can arise from the nonuniform distribution of sources and sinks, short residence times, and the multi-scale nature of interactions between BC, clouds, and atmospheric dynamics — many of which occur on scales smaller than a typical global model grid-box. Past research suggests that discrepancies between aerosol modeling schemes and observations may be attributed to these sub-grid spatial variations [e.g., *Gustafson et al.*, 2011; *Wang et al.*, 2011; *Benkovitz and Schwartz*, 1997].

[4] Previous attempts to quantify scales of variability of aerosols have focused on variability of aerosol radiative properties. *Anderson et al.* [2003] used autocorrelation functions of a number of observational datasets to assess the temporal and spatial variability of aerosol optical properties. These showed that most of the variation in aerosol properties existed on spatial scales of 40–160 km. Analysis of spatial variability of AOD data measured by aircraft campaigns demonstrated that variations in AOD measurements can be as large as 50–70%, but more typically 25–50%, over horizontal distances of 50 km [*Redemann et al.*, 2005]. Other studies with similar results suggest that aerosol optical properties exhibit spatio-temporal variability at scales smaller than model grid-boxes [*Targino et al.*, 2005; *Ram and Sarin*, 2009]. Studies assessing specifically BC scales of variability are scarce; however, a small number have looked at correlations between BC measurements made at nearby sites in populated cities and found BC concentrations to be weakly correlated between sites, suggesting a high degree of spatial variability at neighborhood scales [*Venkatachari et al.*, 2006; *Thornhill et al.*, 2008; *Snyder et al.*, 2010].

[5] This work uses measurements of BC mass from a recent aircraft campaign, HIAPER Pole-to-Pole Observations (HIPPO) [*Schwarz et al.*, 2010b], to quantify the scales of variability of BC plumes. The HIPPO flight track spans thousands of kilometers with nearly continuous vertical profiling in order to provide substantial latitudinal and vertical coverage of BC in the troposphere. This unique dataset allows us to characterize the spatial scales of typical BC plumes in a large region of the globe.

2. Methods

2.1. Aircraft Measurements

[6] The measurements included in the analysis were taken on board the NSF/NCAR GV [hippo.ucar.edu] aircraft during the first three missions of the HIPPO campaign (subsequently referred to as HIPPO1, HIPPO2, and HIPPO3). The flights provide extensive vertical coverage, consisting of over 400 vertical profiles, with altitudes ranging from 0.2 to 14 km, and with a nearly global span of latitudes, ranging from 85°N to 67°S. The three missions took place during different seasons with the first (HIPPO1) occurring during the period of 9–30 January 2009, HIPPO2 from 31 October

[1]Atmospheric, Oceanic and Planetary Physics, Department of Physics, University of Oxford, Oxford, UK.
[2]Cooperative Institute for Research in Environmental Sciences, University of Colorado at Boulder, Boulder, Colorado, USA.
[3]Earth System Research Laboratory, National Oceanic and Atmospheric Administration, Boulder, Colorado, USA.
[4]Science and Technology Corporation, Boulder, Colorado, USA.

Corresponding author: N. M. Weigum, Atmospheric, Oceanic and Planetary Physics, Department of Physics, University of Oxford, Clarendon Laboratory, Parks Road, Oxford OX1 3DR, UK. (weigum@atm.ox.ac.uk)

0094-8276/12/2012GL052127

Table 1. Plume Statistics From HIPPO Campaign

Campaign Mission	Number of Plumes	Median Scale (km)	Total BC Mass (ng)	% Mass in Plumes
All	100	113	12	57
HIPPO1	20	102	1.9	28
HIPPO2	43	121	2.7	56
HIPPO3	37	123	7.5	65

to 22 November 2009, and HIPPO3 from 24 March to 16 April 2010.

[7] BC measurements were made with a Single-Particle Soot Photometer (SP2) [*Schwarz et al.*, 2010b]. The SP2 provides highly sensitive measurements of BC mass and mixing state of individual BC-containing particles. Recent inter-comparisons of instruments measuring BC content of soot aerosol have shown that SP2 measurements of BC mass in individual aerosol particles are independent of particle mixing state and morphology [*Cross et al.*, 2010]. The SP2 data is collected on a per-particle basis so that a particle's mass is recorded each time a particle is detected. For the current analysis, BC mass measurements are averaged over one-second time intervals and converted to a mass mixing ratio (MMR) in ng of BC per kg of dry air with a net uncertainty estimated at 30% in accumulation mode BC mass. Because our interest lies in the spatial scales of BC plumes, the one-second time data is converted to spatial units using the aircraft's true airspeed at each time step so that the BC MMR is described as a function of 'distance along the flight track' with 1-second resolution.

2.2. Plume Identification

[8] To facilitate the identification of major plume structures, the data from each HIPPO flight was smoothed by the regularization method. The concept behind smoothing by regularization is to balance a 'goodness-of-fit' term with the 'roughness' of the approximation using a smoothing parameter. The smoothing parameter is optimized by the generalized cross-validation [cf. *Stickel*, 2010]. Comparison of the power spectral density functions of the smoothed and unsmoothed data shows they diverge at scales less than 10 km. The smoothing therefore imposes a lower bound of 10 km on the identified plumes scales; however, this lower bound does not have a significant impact on the results.

[9] In the context of this analysis, a plume is defined as an occurrence of elevated mass mixing ratio above the background level. Based on this premise, a simple algorithm for plume identification was developed. In the first step, local maxima and minima present in the data are identified. A threshold MMR level for a plume is defined. All maxima above this level are considered plume peaks, and the scale of the plume is quantified by the distance between the two local minima on either side of the peak. Any overlapping plumes are merged into one larger plume. The threshold MMR is used so that only peaks above the background noise level are identified as plumes. As a rough measure of the noise, the threshold MMR level for each mission is set to the standard deviation of BC MMR from that mission, corresponding to values of 13, 11, and 41 ng/kg-air for HIPPO1, HIPPO2, and HIPPO3, respectively. The sensitivity of the plume identification algorithm to the value of the threshold was tested by varying the value from 5 to 50 ng/kg-air for each campaign. The average scale of the identified plumes was found to vary only by 16, 10, and 8% for HIPPO1, HIPPO2, and HIPPO3, respectively.

[10] Because the HIPPO campaign consists of a series of slant vertical profiles, our capability of separating the plume scales into their horizontal and vertical components is limited. As such, the plume scale in this analysis is a 'scale along the (slanted) flight track' rather than a horizontal or vertical scale.

3. Results and Discussion

3.1. Plume Statistics

[11] A total of 112 BC plumes were identified during the campaign. Twelve plumes were located at altitudes less than 2 km and were likely the result of sampling polluted boundary layer air. These plumes are not demonstrative of BC plume scales and are not included in the analysis, leaving a total of 100 plumes. Table 1 provides a summary of the plume statistics from each mission. The plumes encompass a large spread of scales, ranging from 34 km to 648 km, with a median of 113 km. HIPPO1 contains roughly half the number of plumes as HIPPO2 and HIPPO3, and the median plume scale is 20% smaller than HIPPO2 and HIPPO3. This could be due to seasonal, rainfall, source and transport differences between missions. Also note that 57% of the total BC mass from the campaign is found within the identified plumes, highlighting the important contribution of plumes to total BC present in the atmosphere.

[12] Another issue to consider is if BC plumes were distributed in thin vertical layers with continuous horizontal extent, then this analysis method would detect those layers as a series of plumes where the analyzed spatial scale was set by the thickness of the layers and the ratio of the vertical and horizontal speeds. The impact of this artefact is likely small since the majority of plumes were identified during different flights legs and non-consecutive vertical profiles with a variety of peak concentrations and altitudes; however, it could potentially affect some of the identified plume scales and is an acknowledged limitation of the analysis.

3.2. Spatial Distribution of Plumes

[13] Figure 1 shows the locations of the identified plumes. The majority of plumes are located in the Northern Hemisphere in areas over the Pacific Ocean, North Pole and North America, with relatively few plumes in the Southern Hemisphere. This is likely primarily due to the relative lack of BC sources contributing to loadings in the South Pacific Ocean.

[14] Extensive research in pollution transport to the Arctic region has shown that Arctic air masses can be influenced by long-range transport from biomass-burning and anthropogenic source regions at lower latitudes, especially in winter and early spring [*Stohl*, 2006]. Arctic plumes may also arise from injection of BC into the troposphere near its source by local biomass burning events, as was the case for plumes detected during the ARCPAC campaign [*Warneke et al.*, 2009; *Koch et al.*, 2009], which sampled BC plumes in the Alaskan Arctic region in April 2008. These types of sources could have similarly contributed to the presence of the HIPPO Arctic plumes. The large number of HIPPO plumes identified in the North Pacific region are also likely due to similar transport mechanisms. *Holzer et al.* [2005] showed that significant amounts of East Asian air are transported across the Pacific Ocean, particularly from March to August.

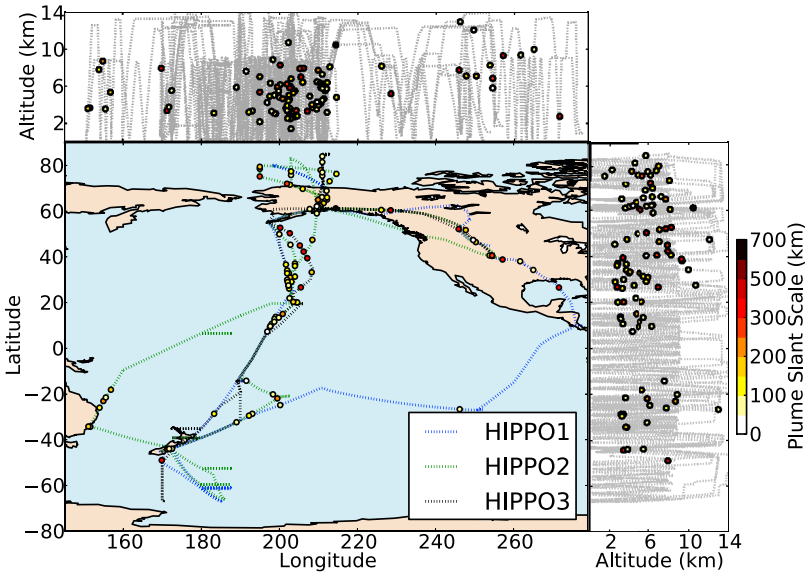

Figure 1. The large center panel shows the location of each plume peak along the flight track of the three HIPPO missions. The right and top panels show the altitudes of the corresponding plume peaks as a function of latitude and longitude, respectively. The gray dotted lines in each side panel represent the flight track of the entire campaign. The colorbar is the plume scale in kilometers.

Schwarz et al. [2010a] attributed northern Asia as a likely source region for the BC detected in HIPPO1.

[15] The side panels of Figure 1 show that most regions contain plumes with a wide range of different scales spanning altitudes from 1 to 13 km. While no distinct pattern is present, the majority of plumes were detected in the mid-troposphere. The different sources and transport mechanisms of BC in these regions contribute to the wide range of observed plume scales. Midlatitude synoptic low pressure systems can carry biomass burning plumes from Asia and Eastern Europe over the Pacific Ocean, and these plumes can be sheared horizontally into fine-scale filaments and layers as they exit the cyclonic systems. These layers have been observed in the free troposphere in both Arctic and Pacific regions in previous observational campaigns [*Brock et al.*, 2011; *Liu et al.*, 2003]. This mechanism may contribute to the large number of small-scale HIPPO plumes observed at mid-tropospheric altitudes.

3.3. Plume Composite

[16] To gain a better understanding of the general characteristics and overall shape of BC plumes, a composite of all plumes is produced by re-gridding the distance along the flight track to distance from plume peak at 0.5 km equal spacing. The composite is then created by determining the median MMR at each 0.5 km interval away from the plume peak. The blue line in Figure 2 depicts the composite of all 100 identified plumes, and the top panel indicates the number of plumes averaged in each 0.5 km bin. Only bins with 20 or more plumes are included in the composite. The plume composite has a clear Gaussian shape, so to quantify its scale, a Gaussian function is fit to the composite peak according to Levenberg-Marquardt least-squares minimization (code developed by Adam Ginsburg, code.google.com/p/agpy/). The scale of the composite plume is approximated to six times the standard deviation of the Gaussian, which encompasses 99.7% of the area under the curve. The Gaussian has a standard deviation of 13 km, and so the scale of the composite plume is approximately 80 km. The composite structure was insensitive to the disparate peak values of the various plumes; normalization of the plumes before compositing did not affect this result. The scale of the composite plume is considerably less than the value of the median plume scale (113 km); however, this is because the composite is more representative of smaller scale plumes. This is visible in Figure 2, which includes the re-gridded HIPPO plumes, centred at their peak. One can see, as the distance from the peak increases, most of the plumes drop off at distances less than 100 km from the peak until only the broader, less Gaussian plumes remain. Because the composite only includes bins with 20 or more plumes, the shape and scale of the composite reflect the high number of small-scale plumes.

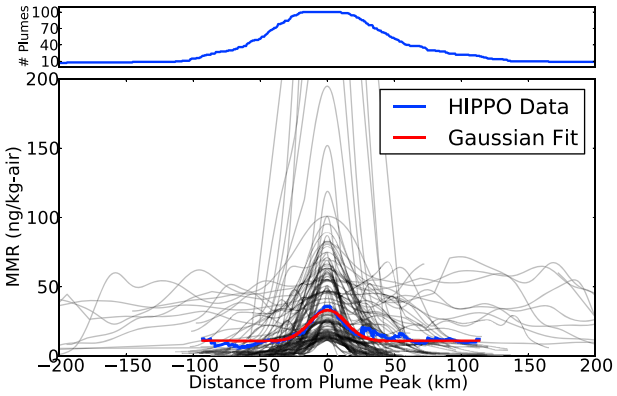

Figure 2. A composite of all plumes is represented by the blue line. The top panel shows the number of plumes included in each composite bin; only bins with at least 20 plumes are depicted in the composite. The red line is a Gaussian fit to the composite. The gray lines represent the individual identified plumes.

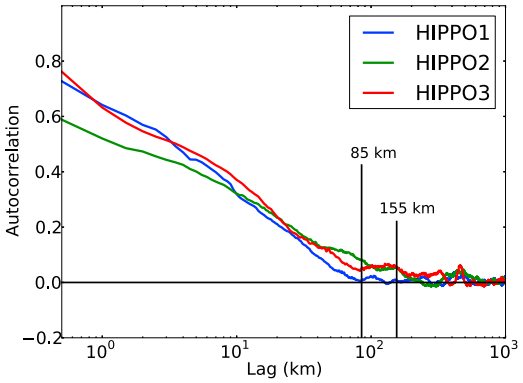

Figure 3. The average daily spatial autocorrelation as a function of lag (in km) for the three HIPPO phases.

3.4. Comparison to Effective Model Resolution

[17] Because the identified plume scales have both horizontal and vertical components, comparing these scales to a GCM's horizontal resolution is an inaccurate way of quantifying a model's ability to resolve these plumes, since this disregards the GCM's vertical resolution. In order to make an accurate comparison between the HIPPO plume scales and typical GCM resolutions, we define an approximate 'effective model resolution', which takes into account the flight track geometry of the HIPPO campaign and the vertical resolution of the model. A typical modern GCM for use in climate modelling has a horizontal grid spacing of 1–2° (100–200 km at the equator) and a vertical grid spacing in the range of a few hundred meters up to a kilometer (at altitudes in the range of the identified plumes). To calculate an 'effective model resolution' we use the slope of each vertical profile from HIPPO and the height of a typical tropospheric vertical level in a GCM (varied from 300 m to 1 km) to calculate the total distance traveled through a grid box. These distances vary from 4 km for the lowest altitudes and steepest slopes to 58 km for higher altitudes and shallower climbs. If we approximate the minimum resolvable wavelength of a numerical model to be four times the model grid spacing, then the effective model resolution is anywhere in the range of approximately 20–230 km. Eight-three percent of the identified plumes (62% of the mass) are smaller or of similar magnitude to this range.

3.5. Autocorrelation Analysis

[18] To relate this work to previous attempts to quantify aerosol scales of variability, autocorrelation analysis is performed on the unsmoothed data from each HIPPO mission, in a manner similar to *Anderson et al.* [2003]. Figure 3 shows the average daily spatial autocorrelation for each HIPPO campaign as a function of lag (in kilometers). The autocorrelation functions were derived from the power spectral density distributions using the Wiener-Khinchin theorem. The autocorrelation of all three missions drops off rapidly, with HIPPO1 reaching a plateau of nearly zero correlation at a lag of 85 km and HIPPO2 and HIPPO3 reaching a near-zero plateau at 155 km, after which the three curves become rather noisy. This signifies that most of the BC variability exists at scales below 85–155 km. These scales are of similar magnitude to the along-track scales of the HIPPO plumes, suggesting that a large degree of BC variability is accounted for in these plume structures. *Anderson et al.* [2003] found a similar range of scales for the variability of aerosol optical depth (40–160 km). Their analysis included spaceborne lidar data and aircraft data from level segments of flight legs, ensuring that their measured scales of variability represent strictly horizontal scales. Because of the nature of the HIPPO flights, the data is unable to be separated into horizontal and vertical components; however, the agreement between HIPPO scales of variability and those determined by *Anderson et al.* [2003] suggests that the HIPPO scales have a substantial horizontal component.

4. Summary and Implications

[19] In this study, we quantify the scales of variability of BC plumes identified during the first three missions of the HIPPO aircraft campaign, and determine how these scales relate to current GCM resolutions used in climate modeling simulations. A total of 100 plumes were identified during the campaign. These plumes represent a large portion (57%) of the total mass of BC measured during the campaign, confirming that these plumes represent important features of BC in the atmosphere. The plume statistics show that the median plume scale is 113 km. A plume compositing technique, which reflects the high number of small-scale plumes, reveals that a typical BC plume has a Gaussian shape and a scale of approximately 80 km. From these two analyses, we can infer that a typical BC plume scale is in the range of 80–110 km. Autocorrelation analysis reveals that most of BC's variability occurs on scales smaller than 85–155 km, which is similar in magnitude to previous studies of aerosol horizontal variability. This range of total BC variability overlaps considerably with the range of BC plume scales, suggesting that most of the BC variability can be accounted for by these plume structures.

[20] Comparing the along-flight-track scale to an 'effective model resolution', we are able to show that most of the plumes exist on scales that are smaller or of similar magnitude to the effective model resolution, which ranges from 20 km for low altitudes and steep ascents to 230 km for high altitudes and shallower ascents. Large-scale plumes (>230 km) and plumes located at low altitudes with significant vertical structure are likely resolvable by a typical GCM; however, plumes representing horizontal features at these scales are too small to be captured by GCMs running at climate modeling resolutions. The agreement between HIPPO scales of variability and previous calculations of horizontal aerosol variability, suggests that the HIPPO plumes have a significant horizontal component. Although the identified plume scales are roughly half the size of GCM resolutions, the capabilities of GCMs are rapidly increasing, and running climate model simulations at twice the resolution will likely be possible in the near future. Because BC plumes represent a large portion of total BC in the atmosphere and account for a large degree of its variability, it is crucial for aerosol models to capture these features in order to accurately describe BC's effect on radiative forcing and the climate.

[21] **Acknowledgments.** This work was supported by the Natural Sciences and Engineering Research Council of Canada, the Clarendon Fund, and by the UK Natural Environment Research Council project AEROS [NE/G006148/1]. Data was provided by NCAR/EOL under sponsorship of the National Science Foundation. http://data.eol.ucar.edu/.

[22] The Editor thanks two anonymous reviewers for assisting in the evaluation of this paper.

References

Anderson, T. L., R. J. Charlson, D. M. Winker, J. A. Ogren, and K. Holmen (2003), Mesoscale variations of tropospheric aerosols, *J. Atmos. Sci.*, *60*(1), 119–136.

Bauer, S. E., S. Menon, D. Koch, T. C. Bond, and K. Tsigaridis (2010), A global modeling study on carbonaceous aerosol microphysical characteristics and radiative effects, *Atmos. Chem. Phys.*, *10*(15), 7439–7456, doi:10.5194/acp-10-7439-2010.

Benkovitz, C. M., and S. E. Schwartz (1997), Evaluation of modeled sulfate and SO_2 over North America and Europe for four seasonal months in 1986–1987, *J. Geophys. Res.*, *102*(D21), 25,305–25,338.

Brock, C. A., et al. (2011), Characteristics, sources, and transport of aerosols measured in spring 2008 during the Aerosol, Radiation, and Cloud Processes Affecting Arctic Climate (ARCPAC) project, *Atmos. Chem. Phys.*, *11*(6), 2423–2453, doi:10.5194/acp-11-2423-2011.

Cross, E. S., et al. (2010), Soot particle studies instrument inter-comparison project overview, *Aerosol Sci. Technol.*, *44*(8), 592–611, doi:10.1080/02786826.2010.482113.

Gustafson, W. I., Jr., Y. Qian, and J. D. Fast (2011), Downscaling aerosols and the impact of neglected subgrid processes on direct aerosol radiative forcing for a representative global climate model grid spacing, *J. Geophys. Res.*, *116*, D13303, doi:10.1029/2010JD015480.

Holzer, M., T. M. Hall, and R. B. Stull (2005), Seasonality and weather-driven variability of transpacific transport, *J. Geophys. Res.*, *110*, D23103, doi:10.1029/2005JD006261.

Koch, D., et al. (2009), Evaluation of black carbon estimations in global aerosol models, *Atmos. Chem. Phys.*, *9*(22), 9001–9026.

Liu, H., D. J. Jacob, I. Bey, R. M. Yantosca, B. N. Duncan, and G. W. Sachse (2003), Transport pathways for Asian pollution outflow over the Pacific: Interannual and seasonal variations, *J. Geophys. Res.*, *108*(D20), 8786, doi:10.1029/2002JD003102.

Ram, K., and M. M. Sarin (2009), Absorption coefficient and site-specific mass absorption efficiency of elemental carbon in aerosols over urban, rural, and high-altitude sites in India, *Environ. Sci. Technol.*, *43*(21), 8233–8239, doi:10.1021/es9011542.

Ramanathan, V., and G. Carmichael (2008), Global and regional climate changes due to black carbon, *Nat. Geosci.*, *1*(4), 221–227, doi:10.1038/ngeo156.

Redemann, J., et al. (2005), Suborbital measurements of spectral aerosol optical depth and its variability at subsatellite grid scales in support of CLAMS 2001, *J. Atmos. Sci.*, *62*(4), 993–1007.

Schulz, M., et al. (2006), Radiative forcing by aerosols as derived from the AeroCom present-day and pre-industrial simulations, *Atmos. Chem. Phys.*, *6*, 5225–5246.

Schwarz, J. P., J. R. Spackman, R. S. Gao, L. A. Watts, P. Stier, M. Schulz, S. M. Davis, S. C. Wofsy, and D. W. Fahey (2010a), Correction to "Global-scale black carbon profiles observed in the remote atmosphere and compared to models," *Geophys. Res. Lett.*, *37*, L23804, doi:10.1029/2010GL046007.

Schwarz, J. P., et al. (2010b), The detection efficiency of the single particle soot photometer, *Aerosol Sci. Technol.*, *44*(8), 612–628, doi:10.1080/02786826.2010.481298.

Snyder, D. C., A. P. Rutter, C. Worley, M. Olson, A. Plourde, R. C. Bader, T. Dallmann, and J. J. Schauer (2010), Spatial variability of carbonaceous aerosols and associated source tracers in two cites in the midwestern United States, *Atmos. Environ.*, *44*(13), 1597–1608, doi:10.1016/j.atmosenv.2010.02.004.

Stickel, J. J. (2010), Data smoothing and numerical differentiation by a regularization method, *Comput. Chem. Eng.*, *34*(4), 467–475, doi:10.1016/j.compchemeng.2009.10.007.

Stohl, A. (2006), Characteristics of atmospheric transport into the Arctic troposphere, *J. Geophys. Res.*, *111*, D11306, doi:10.1029/2005JD006888.

Targino, A. C., K. J. Noone, and E. Ostrom (2005), Airborne in situ characterization of dry aerosol optical properties in a multisource influenced marine region, *Tellus, Ser. B*, *57*(3), 247–260.

Thornhill, D. A., et al. (2008), Spatial and temporal variability of particulate polycyclic aromatic hydrocarbons in Mexico City, *Atmos. Chem. Phys.*, *8*(12), 3093–3105.

Venkatachari, P., L. Zhou, P. K. Hopke, D. Felton, O. V. Rattigan, J. J. Schwab, and K. L. Demerjian (2006), Spatial and temporal variability of black carbon in New York City, *J. Geophys. Res.*, *111*, D10S05, doi:10.1029/2005JD006314.

Wang, M., et al. (2011), The multi-scale aerosol-climate model PNNL-MMF: Model description and evaluation, *Geosci. Model Dev.*, *4*(1), 137–168, doi:10.5194/gmd-4-137-2011.

Warneke, C., et al. (2009), Biomass burning in Siberia and Kazakhstan as an important source for haze over the Alaskan Arctic in April 2008, *Geophys. Res. Lett.*, *36*, L02813, doi:10.1029/2008GL036194.